J Mater Sci (2009) 44:6040–6053
DOI 10.1007/s10853-009-3828-6

Investigation of pseudocapacitance effect and frequency dependence of ac impedance in polyaniline–polyoxometalate hybrids

P. Chithra lekha · S. Subramanian · D. Pathinettam Padiyan

Received: 18 April 2009 / Accepted: 20 August 2009 / Published online: 3 September 2009

Abstract In polyaniline (PAni) prepared by interfacial polymerization, the conductivity increases with temperature due to the heating induced molecular arrangement which is favorable for charge delocalisation. The hydroxyl groups present in the polyoxometalates-doped PAni hybrids play a vital role in the conductivity mechanism of these materials. The appearance of pseudocapacitance loop at low frequency region is due to the temperature-assisted formation of oxonium ions and the protonation of polymer by this at the electrode–electrolyte interface and it is in agreement with the TGA studies. From the frequency dependant conductivity measurements at high temperatures, it is found that, PAni obeys the correlated barrier hopping model whereas its hybrids follow overlapping large polaron tunneling model.

Introduction

Impedance spectroscopy is a powerful tool for characterizing the electrical properties of materials having various conducting species. It may be used to investigate the dynamics of bound and mobile charges in bulk or interfacial regions of any kind of solid or liquid material [1]. Conducting polymers are highly disordered materials for which the enhancement of conductivity on doping/dedoping comes from the generation of extended states in doped molecules correlating charged defects with electronic structures. In these materials, the phonon-assisted inter-soliton hopping of electrons between charged and neutral soliton states in the mid gap is explained by using Kivelson approach with ac conductivity technique [2, 3]. Polyoxometalates (POMs) when doped in conducting polymers increase the homogenous charge separation on the polymer by the delocalization of its own negative charges and aid the transfer of charge between the polymer chains. Electrodes based on conductive polymers such as polyaniline (PAni), polythiophene, and polypyrrole (PPY) give rise to pseudocapacitance. Due to this property, PPY doped with POMs is used as supercapacitors by White et al. [4]. PAni—a highly disordered material when doped with crystalline POMs yields a complicated electronic structure. To understand the conduction mechanism in such materials, the impedance spectroscopy is employed since such study is necessary both from the fundamental as well as technological point of view.

P. Chithra lekha · D. Pathinettam Padiyan (✉)
Department of Physics, Manonmaniam Sundaranar University, Tirunelveli 627-012, India
e-mail: dppadiyan@sancharnet.in

S. Subramanian
Department of Physics, The MDT Hindu College, Tirunelveli 627-010, India

Experiment

Aniline monomer, chloroform, HCl, and ammonium peroxydisulphate used were of analytical grade from E. Merck. Aniline was distilled prior to use and the double distilled water was used throughout the experiment. The POMs, 12-tungstophosphoric acid (12TPA), 11-tungsto 1-vanadophosphoric acid (11TPA), 12-molybdophosphoric acid (12MPA), and 11-molybdo 1-vanadophosphoric acid (11MPA) were prepared by the ether extraction method. In a typical synthesis, to the organic solution prepared by dissolving 0.625 M aniline monomer in chloroform, the aqueous solution of 0.16 M ammonium peroxydisulphate in 1 M HCl was added, generating an interface where a thin layer of green PAni nanomaterial appears. During the oxidative polymerization of aniline, HCl acts as proton source and

provides necessary counter ions to the developing charged polyaniline. As the aniline monomer is protonated on the surface, its head to tail coupling forms a low-energy helical structure when polymerized and precipitated into aqueous phase of the biphasic system. After 2 h, the PAni was filtered using Buchner funnel, washed with ethanol and water to remove unreacted chemicals and aniline oligomers, oven dried and the nano PAni was collected. The preparation of PAniPOM nanocomposites were made by replacing the protonic acid HCl with the subsequent POM. Here the POM acts as a proton source as well as a dopant.

The characterization of PAni and PAniPOMs are done with interfacial polymerization and the procedure is given elsewhere [5]. The thermal analysis for PAni and PAniPOMs were done with the Perkin Elmer Diamond thermal analysis system in the nitrogen atmosphere at a constant heating rate of 5 °C/min in non-isothermal condition. The polymer powder is pelletized at a constant pressure of 2 tons using hydraulic pellet press. The ac impedance analysis on 13 mm diameter pellets of PAni and its hybrids are done with Lock-in Amplifier model SR830 in the frequency range 10–100 kHz at temperatures ranging from room temperature to 398 K with copper electrodes.

Results and discussion

Thermal analysis

The TGA thermogram for PAni shown in Fig. 1a have three step weight loss as follows: the loss of water molecules (25–85 °C), the loss of HCl and aniline oligomers (143–315 °C), and the destruction of the skeletal backbone of PAni (318–632 °C). In the DTA of PAni, there are three endothermic peaks at 54, 309, and 510 °C indicating the consecutive weight loss stages as discussed in TG.

In the case of P12MPA and P12TPA, the complete process of weight loss is composed of four stages namely,

- the dehydration from PAni and POMs
- decomposition of aniline oligomers and/or dehydration of the water of crystallization of POMs
- decomposition of anions of POMs
- decomposition of PAniPOM complexes and the depolymerization of PAni

In the Fig. 1, four major weight loss stages for P12MPA are observed at I: 26–85 °C, II: 200–335 °C, III: 385–580 °C, and IV: 600–810 °C. The DTA of P12MPA shows six endothermic peaks at 30, 115, 225, 375 575, and 710 °C among which the first two are peaks of dehydration, third indicates the dehydration of the water of crystallization of P12MPA, and the fourth one is due to the decomposition of aniline oligomers. The P12TPA also has a four

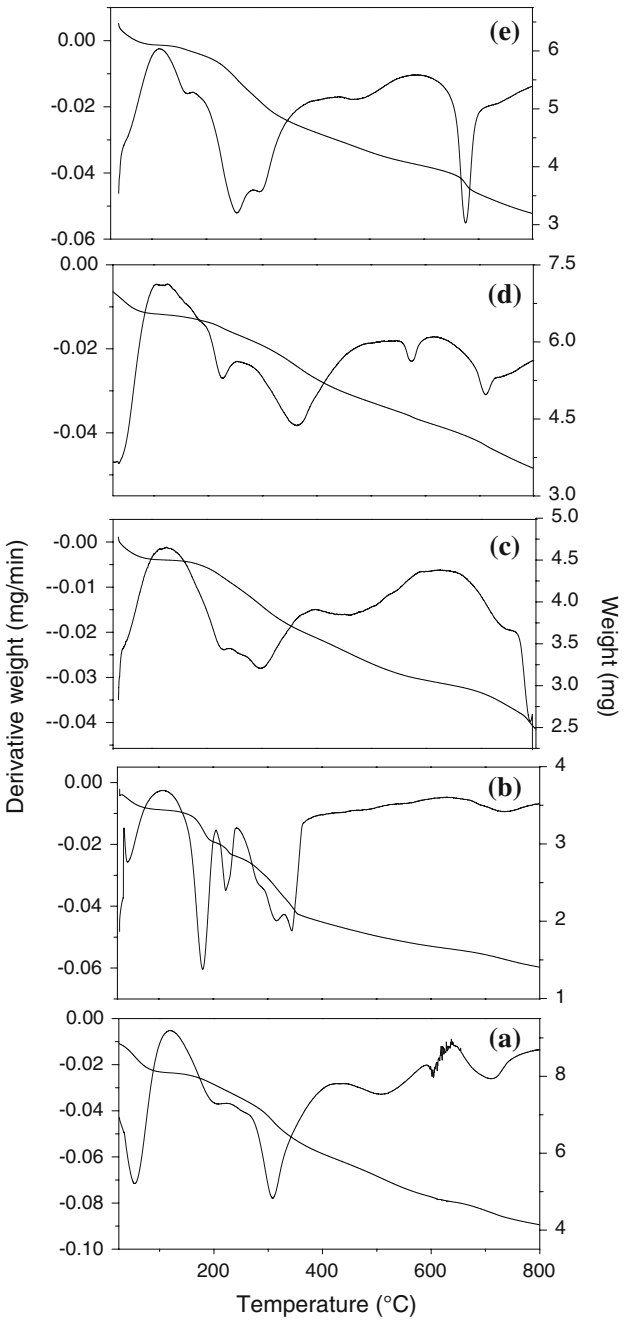

Fig. 1 TG-DTA curve for **a** PAni, **b** P12TPA, **c** P11TPA, **d** P12MPA, **e** P11MPA

step weight loss at I: 35–70 °C, II: 165–195 °C, III: 240–355 °C, and IV: 355–700 °C which is quite different from the thermal behavior of the other PAniPOMs. In P12TPA, the DTA has six endothermic peaks at 45, 182, 226, 742, and a doublet at 311 and 348 °C. It is found that the weight loss in P12MPA at different temperatures is slow compared to that of P12TPA and indicates its higher stability. The percentage of weight loss in P12TPA is higher than the pristine PAni and other PAniPOMs. The number of water

molecules lost during dehydration stage in PAni is found to be two whereas in P12TPA it is 16 in the dehydration region among this 15 are the water of hydration present in 12TPA. The Rosenheim's dehydration experiment showed that the water of crystallization of POMs are easily expelled from crystals at moderate temperatures, but the appropriate number of constitutional water molecules are expelled only at much higher temperatures accompanied by the disintegration of the complexes [6]. According to Nakamura et al. [7], in 12MPA, the dehydration of all the molecules (29 H_2O) of water of crystallization is around 100 °C whereas the tungsten analog dehydrates water of crystallization around 100 °C and the remaining six water molecules expelled around 200 °C. In the TGA of P12TPA, the additional shoulder seen in between the decomposition of aniline oligomers and decomposition of anions of POMs at 195–240 °C is attributed to the expulsion of the six water molecules. Usually, at moderate temperatures, the 12TPA has the highest thermal stability than the 12MPA, but the thermally decomposed molybdenum POMs can be reconstructed under exposure to water vapor whereas it is not possible in the case of its tungsten analog due to the contribution of these six hydrates. In P12MPA within the dehydration region eight water molecules are lost.

The P11TPA has five step weight loss: I (43–80 °C)—dehydration, II (195–340 °C)—dehydration of water of crystallinity and expulsion of aniline oligomers, III (340–545 °C)—disintegration of 11TPA anions, IV (550–680 °C)—decomposition of polyaniline-11TPA complex, and V (680–770 °C)—depolymerization. The number of water molecules expelled during dehydration in the first stage is calculated as ten in P11TPA. The DTA of this P11TPA has five moderate endothermic peaks at 50, 232, 300, 460, and 740 °C. The thermal degradation of the vanadium substituted P11MPA also exhibits five weight loss stages: I (40–85 °C)—dehydration in which nine water molecules are lost; II (140–220 °C)—dehydration of water of crystallinity; III (225–320 °C)—the expulsion of aniline oligomers; IV (355–560 °C)—disintegration of 11MPA anions, and V (680–805 °C)—decomposition of P11MPA complex and the depolymerization of PAni as shown in Fig. 1. The DTA shows endothermic peaks at 50, 164, 257, 478, and 677 °C among which the peak at 257 °C is a doublet. The replacement of molybdenum with a vanadium ion in molybdophosphoric acid has affected the thermal behavior of the composite. When addenda atoms present in the Keggin structure of 12MPA and 12TPA is replaced in the order with the incorporation of one vanadium, which is a lower valent transition ion, the degradation of the polymer/inorganic nanomaterial gets affected and leads to multiple step degradation process.

Integral procedural decomposition temperature

In thermogravimetric analysis, there are two types of procedural decomposition temperatures: Differential Procedural Decomposition Temperature (DPDT) and Integral Procedural Decomposition Temperature (IPDT). DPDT means defining the locations of knees in normalized data records whereas IPDT is nothing but summing up the whole shape of the normalized data curve. Since DPDT neither consistently available nor unique, the IPDT is used here. For example, as shown in Fig. 2, one can easily sum up all the dips and meanderings by measuring the area under the curve. The area of the entire crosshatched region in Fig. 2 divided by the area of the total rectangular plotting area provides the total curve area A^* which is normalized with respect to both residual weight and temperature. IPDT values represent the intrinsic thermal stability of the polymer [8]. From Fig. 2 the end-of-volatilization temperature (T_{A^*}) is obtained from the relation,

$$T_{A^*} = 775A^* + 25$$

In this equation, 775 is the temperature at which the reaction stops and the 25 is the room temperature. Since most of the materials begin to decompose at much lower temperature a second curve area, K^* is defined as shown by doubly crosshatched area in Fig. 2. The K^* is the ratio between the doubly crosshatched area and the rectangular area bounded by the characteristic end-of-volatilization temperature and the residual weight fraction at the fixed end-of test temperature, 800 °C. The IPDT determined by

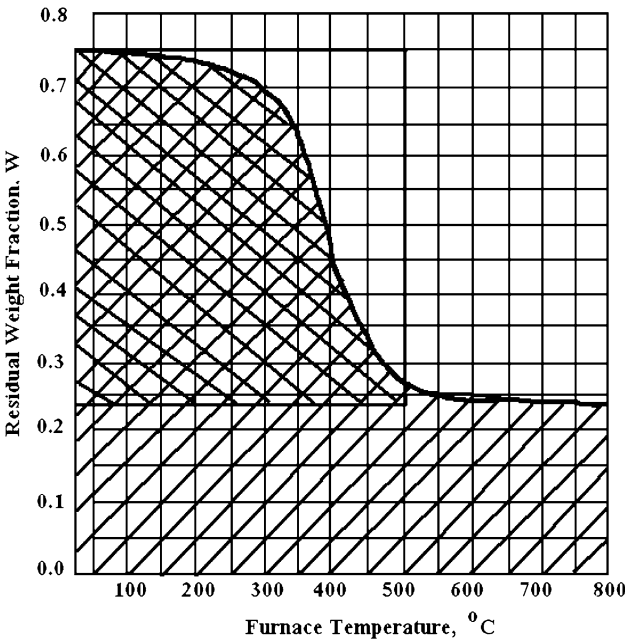

Fig. 2 Thermogram areas, A^* and K^*

Table 1 TG data for PAni and PAniPOM nanomaterials

Sample	Temperature at different weight loss ± 2 (°C)						Oxidation index	IPDT ± 1 (°C)	
	T_0	T_5	T_{10}	T_{20}	T_{50}	T_{max}		T_{A^*}	$T_{A^*K^*}$
PAni	26	60	170	290	715	800	3.2697	570	179
P12TPA	29	55	165	220	472	830	2.5711	477	181
P11TPA	40	80	230	328	801	801	3.6211	602	217
P12MPA	26	67	225	356	799	811	3.4958	600	210
P11MPA	40	80	218	294	783	806	3.4307	580	192

T_0 temperature of onset decomposition, T_5 temperature of 5% weight loss, T_{10} temperature of 10% weight loss, T_{20} temperature of 20% weight loss, T_{30} temperature of 30% weight loss, T_{50} temperature of 50% weight loss, T_{max} temperature at which decomposition completes, T_{A^*} end-of-volatilization temperature, $T_{A^*K^*}$ half volatilization temperature

substituting A^*K^* for A^* in the above equation provides the half volatilization temperature.

The TG data for PAni and various PAniPOMs along with the IPDT and the Oxidation Index (OI) calculated based on the weight of carbonaceous char [9] are given in Table 1 from which the thermal stability of the nanomaterial on doping with various POMs is analyzed. The thermal stability of PAni and all other PAniPOMs except P12TPA are very close. In general, the POMs are thermally unstable at higher temperature. But doping with the PAni has improved its stability and the thermal characteristics of the parent material (PAni) have the power over the thermal property of these polymer/inorganic nanomaterial. The half volatilization temperatures calculated based on IPDT indicate the multiple step decomposition process of the pristine and hybrid materials. It is concluded that except for P12TPA, the observed OI values for all other materials show their good flame retardation.

AC conductivity

The ac impedance spectra for PAni measured at temperatures ranging from 300 to 398 K in the frequency region 10 Hz–100 kHz are shown in Fig. 3. The capacitive and resistive components in the ac impedance data contribute to the semi circles of the Nyquist diagram. In PAni, the plot shows a single semi circle indicating a single relaxation process at room temperature. However, slight variation from the ideality occurred causing depression of the semi circle and deviation of measured points from the semi circle. A semi circle characteristic of an RC equivalent circuit is noticed at all temperatures along with pseudocapacitance loop at low frequency region. In general, the inward or outward folding in the Nyquist plot at low frequency region is attributed to the pseudocapacitance effect in materials. Pseudocapacitance of an electrode is recognized when accepted or delivered charge, q, is faradaic and is a function of potential V. Here charge originates from a faradaic electron transfer process involving a potential-dependant change of oxidation state and sometimes of chemical phase of the surface of the electrode material. The pseudocapacitance arouse from potential dependence of surface coverage by faradaically deposited atomic or radical species like H, OH, or O at the electrode surfaces or from the charging and discharging of conducting polymers such as PAni, PPY, polythiophene, and their derivatives [10–20]. The charging process in conducting polymer is considered as a Lewis acid/base oxidation reaction, the extents of which change with potential giving rise to pseudocapacitance as for surface redox systems. On charging, the polymer chains acquire conductivity due to conjugation, and this charging behavior is equivalent to that of a one-dimensional double layer with the induction of charge analogous to doping of a semiconductor [10]. As the temperature rises a shift of the low frequency region towards the lower resistance is observed in the Nyquist plot of PAni. It shows that the resistivity of PAni decreases with the rise in temperature. The imaginary component reaches to zero indicates that the electrodes are non-blocking type. A non-blocking interface is generally thermodynamically reversible. From the Nyquist plot the bulk conductivity (σ_b) is obtained for all the temperatures using the equation $\sigma_b = \frac{t}{R_b A}$, where t is the thickness and A the area of the electrode and given in Table 2.

The temperature-dependant conductivity value for PAni reveals that, the conductivity increases with temperature. The increase in conductivity with increase in temperature is the characteristic of 'thermal-activated behavior' [21, 22]. Due to the increased efficiency of charge transfer between polymer chains with the increase in temperature may have caused the increase in conductivity or due to effect of thermal curing which affects the chain alignment, leads to the increase of conjugation length of polymer chain. On heating, there will be molecular rearrangement which is also favorable for charge delocalization.

The Nyquist plot of P12TPA (Fig. 4) shows a single semi circle with outward folding in the lower frequency region at room temperature due to pseudocapacitance loop.

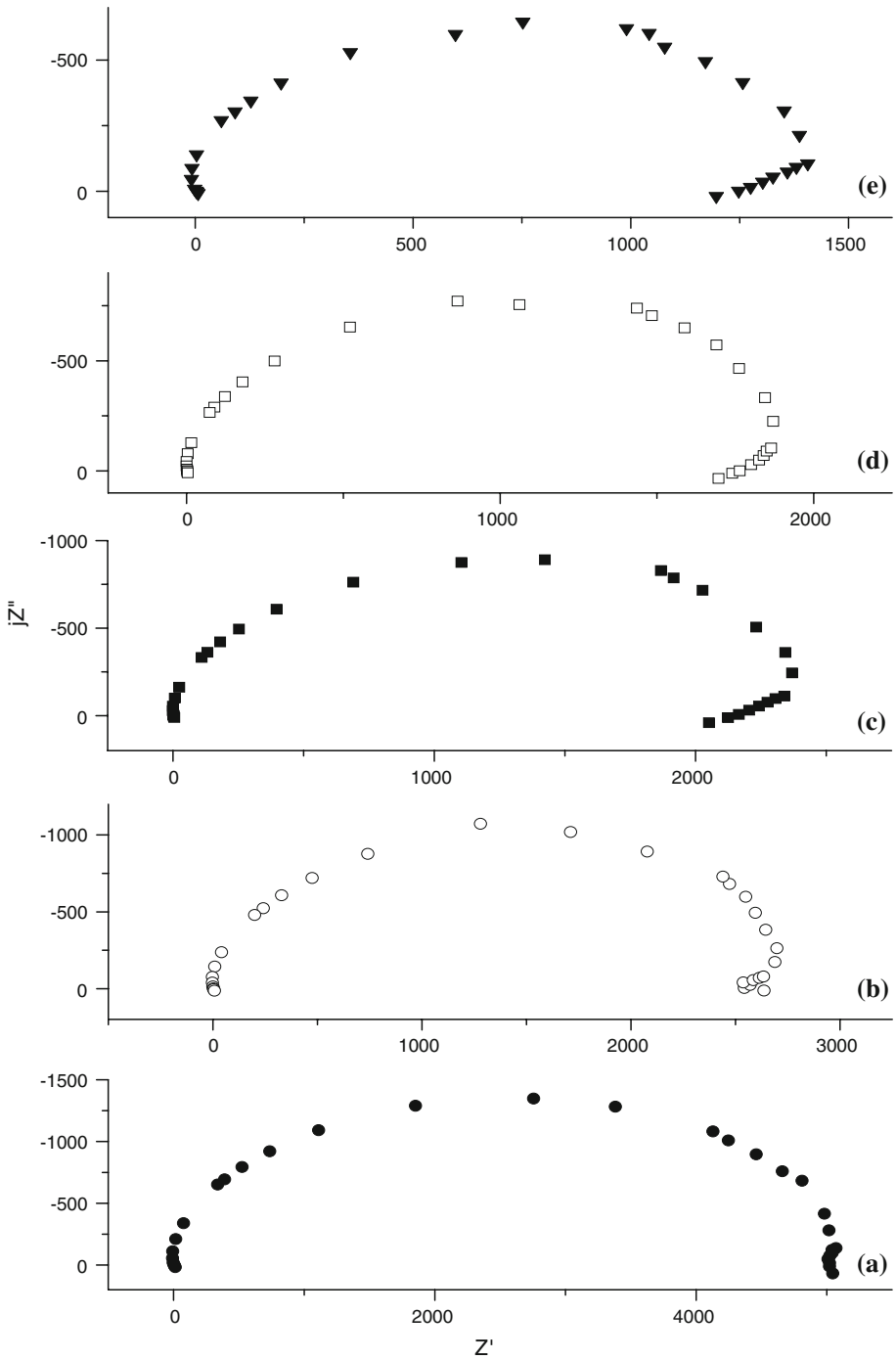

Fig. 3 Nyquist plots for PAni at temperatures **a** 300 K, **b** 323 K, **c** 348 K, **d** 373 K, and **e** 398 K

On increasing the temperature this stretch becomes normal at 373 K and then on further increase in temperature it folds inward which is caused by the pseudocapacitance which is in parallel combination with the RC element. The P12TPA comprises of continuous network of conducting fibrils between which are less conducting regions [23]. The conductivity of P12TPA increases on raising the temperature upto 348 K and afterwards decreases for further increase in temperature. The empirical bulk conductivity of P12TPA shown in Table 2 is much more than PAni. The higher room temperature conductivity in P12TPA compared to PAni is attributed to the protons and other ions in the 12TPA.

In Fig. 5a, the Nyquist plot for P11TPA at room temperature illustrates a single semi circle, showing a single relaxation process. A small distortion is seen at the tail of low frequency region due to spatial charges. This distortion becomes more visible on increasing the temperature

Table 2 Conductivity (σ), depression angle (α), and frequency exponent (s) for PAni and PAniPOMs at different temperatures

T (K)	$\sigma \times 10^{-3}$ (S/m)					α					s				
	PAni	P12TPA	P11TPA	P12MPA	P11MPA	PAni	P12TPA	P11TPA	P12MPA	P11MPA	PAni	P12TPA	P11TPA	P12MPA	P11MPA
300	1.48	7.20	0.89	1.41	0.56	0.201	0.148	0.479	0.271	0.188	0.90(2)	0.60(1)	0.80(3)	0.72(3)	0.84(4)
323	2.92	12.41	1.43	1.70	1.61	0.213	0.119	0.452	0.365	0.335	0.87(2)	0.59(3)	0.78(2)	0.70(4)	0.73(3)
348	3.53	13.10	1.74	2.86	1.51	0.282	0.218	0.299	0.397	0.316	0.70(3)	0.55(2)	0.72(4)	0.63(3)	0.69(2)
373	4.31	10.75	1.85	1.72	0.60	0.171	0.229	0.499	0.548	0.551	0.61(2)	0.60(2)	0.76(3)	0.68(3)	0.80(3)
398	5.98	8.14	1.07	1.55	0.39	0.137	0.197	0.375	0.591	0.659	0.54(4)	0.63(3)	0.81(3)	0.71(3)	0.85(4)

(Fig. 5b–e), which culminates in inward folding of the tail as seen in PAni and P12TPA because of the pseudocapacitance. The conductivity increases until the temperature reaches 348 K and then decreases authenticating the role of hydroxyl group in the conductivity of this hybrid material. From Table 2, it is found that the conductivity of P11TPA is less than that of PAni and P12TPA. The inclusion of lower valent vanadium has decreased the conductivity of the hybrid.

The impedance plot of P12MPA at room temperature (Fig. 6a) has a single semi circle with a lower frequency tail due to the space charges. This tail becomes more distorted on raising the temperature (Fig. 6b, c) and disturbs the shape and symmetry of the semi circle. Above 348 K, the shape of semi circle becomes more depressed and the pseudocapacitance loop appears. At 398 K, the high frequency region stretches and there is a visible depression in the semi circle with lower frequency tail trying to curl inward. The conductivity of P12MPA, increases on raising the temperature upto 348 K and then decreases for further increase as that of the other hybrids.

Figure 7 shows the Nyquist plot of P11MPA and it is analogous to P12MPA. The effect of space charges is visible at low frequency region of Fig. 7a as in other samples. As the temperature is increased, more symmetric semi circle is obtained (Fig. 7b). In Fig. 7c–e, along with the grain boundary impedance the pseudocapacitance loop is noted.

The conductance of a polycrystalline material contains three components which are grain interior, the grain core and a region next to the grain boundaries which is dominated by space charges [24, 25]. Usually this space charge extends over a length called Debye length from the core. The grain boundary impedance arouse because of the random orientation of grains having two-dimensional conductivity. Nanomaterials have large grain boundary area and heterophase interface and there will be a significant increase in the concentration of charge defects which contributes to the conductivity. The domination of large grain boundary arcs in all samples is due to this continuous grain boundary phase. In case of polymolybdates doping, as the temperature is raised, the grain boundaries become discrete and the effect of grain interior amounts only to a distortion of the original arc.

The increase in conductivity of PAni composites can be explained on the basis of proton exchange mechanism between the polymer and the water molecules in the POMs. The mechanism of oxidation and reduction is an important phenomenon in PAni, which is crucial in deciding the increase or decrease in conductivity. The basic repeat units in PAni are determined by the state of the nitrogen atom and consequently labeled as NH_2^+, NH, N=, NH^+=, and $=N^+=$. The repeat units when present in PAni give rise to

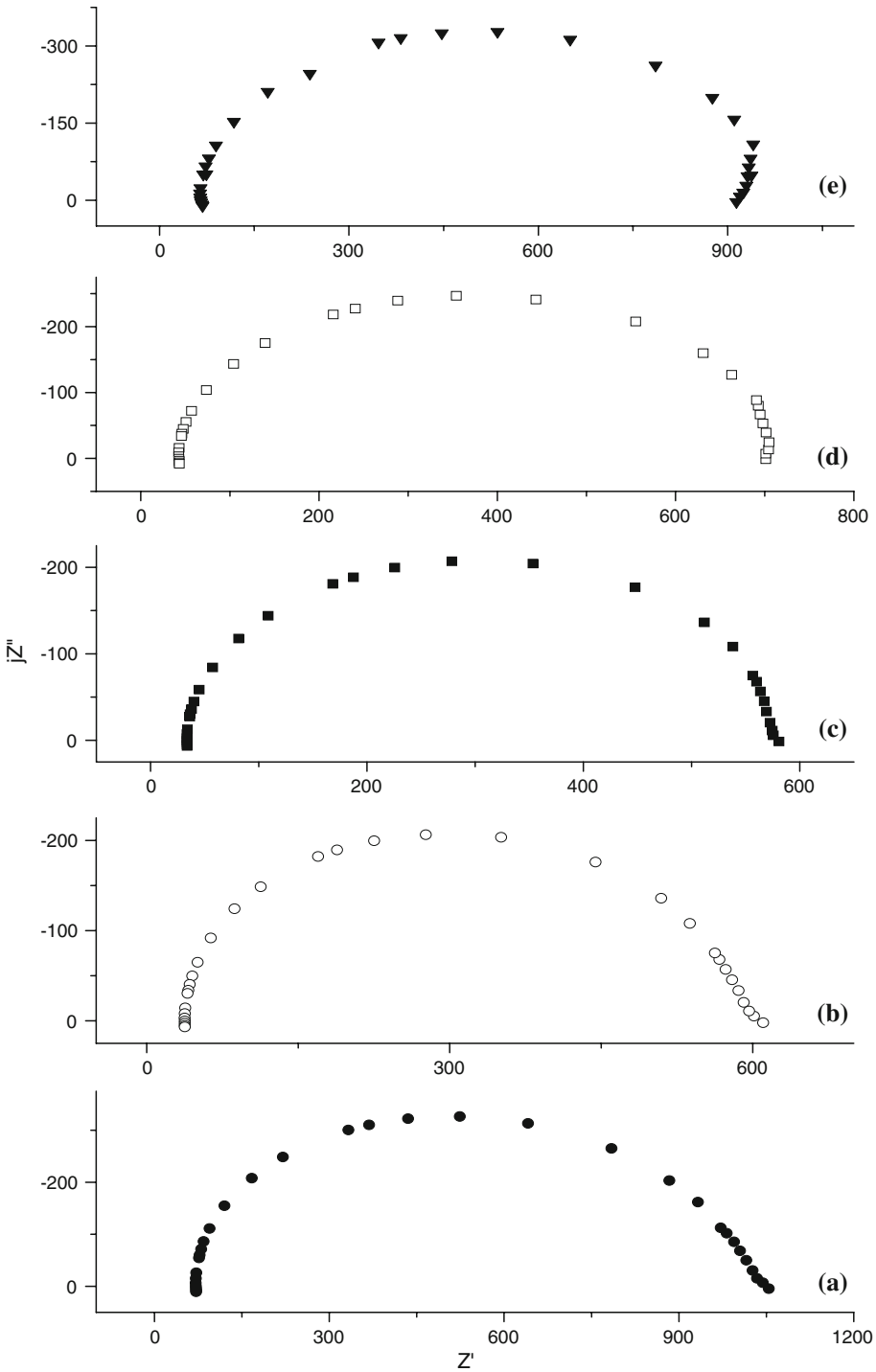

Fig. 4 Nyquist plots for P12TPA at temperatures **a** 300 K, **b** 323 K, **c** 348 K, **d** 373 K, and **e** 398 K

different states. The transformation of one state to the other state occurs due to the oxidation–reduction process. The conduction thus occurs in PAni through hopping of charge carriers by the general process of oxidation. Such protonation can also take place in the presence of water molecules, which can be explained by acid–base reaction. Thus, the water plays a crucial role in the redox mechanism [26, 27]. The spectroscopic results obtained by Mioc et al. [28] for polytungstates and polymolybdates at elevated temperatures show that the water loss is followed by an increase in H_3O^+ ion concentration and that oxonium ion may form dioxonium ion with some of remaining water molecules, i.e.,

$$H_5O_2^+ \leftrightarrow H_3O^+ + H_2O \leftrightarrow -H^+ + 2H_2O$$

This process takes place at the electrode–electrolyte interface and one get the pseudocapacitance during the process as explained earlier. When sample is heated, the

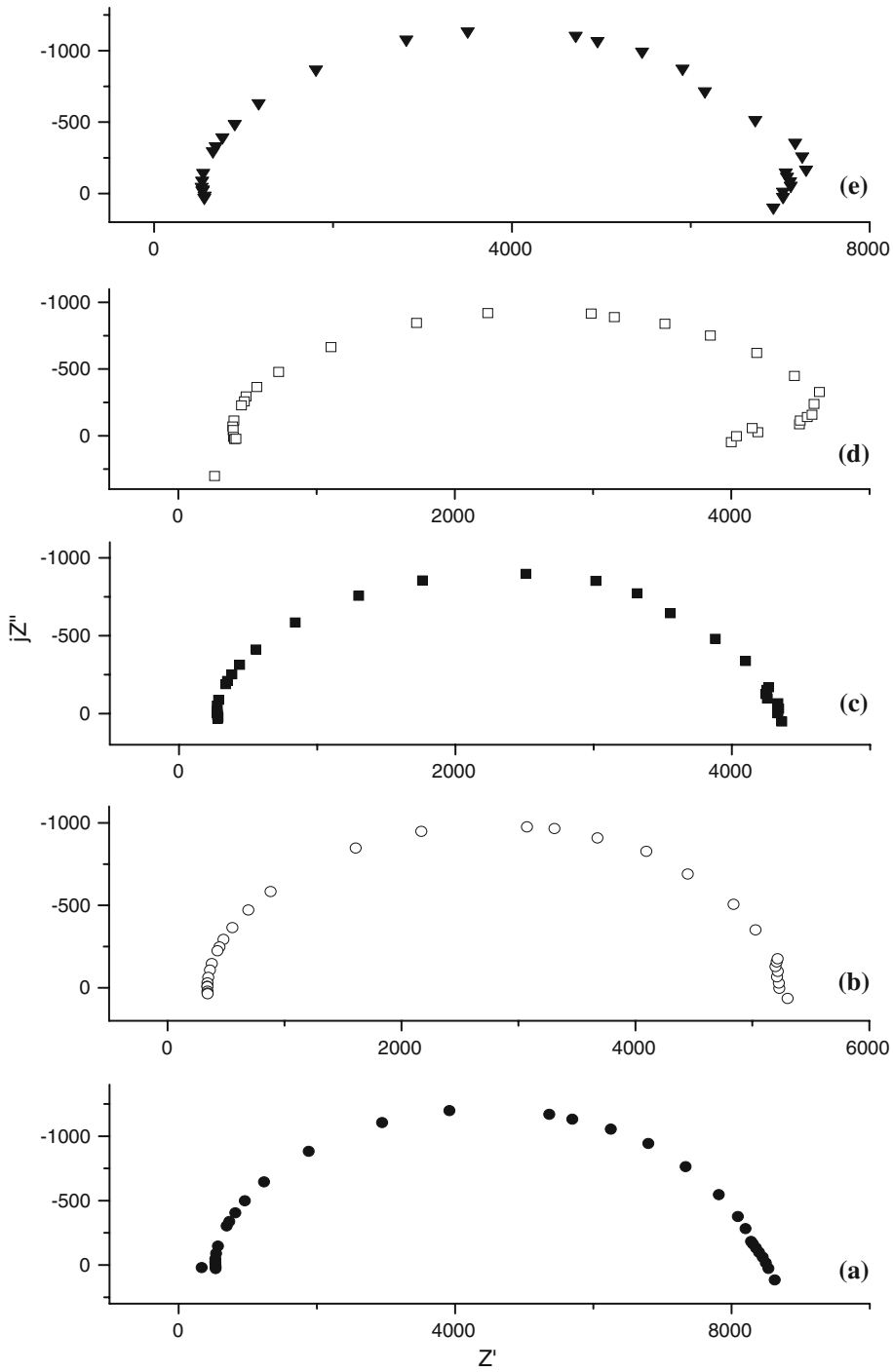

Fig. 5 Nyquist plots for P11TPA at temperatures **a** 300 K, **b** 323 K, **c** 348 K, **d** 373 K, and **e** 398 K

water present in the POMs and polymer form oxonium ions and this may subsequently protonate the polymer. The protonation again produces semiquinone radicals which are charge carriers in PAni and increase the conductivity. This is comparable to the increase in conductivity of PAni on exposing with H_2S reported by Agbor et al. [29]. Upto 348 K, the conductivity increases due to the mobility of charge carriers and protonation of PAni, after which the loosely bound water molecules are dehydrated gradually and the conductivity decreases. TGA studies also show that the water of hydration is more in POMs than PAni and it get expelled as the temperature increases. In PAni–POM hybrid materials, the water molecules present in the POMs play an important role in the conductivities of these materials and as a result the conductivity falls above 348 K. It indicates that the hydroxyl group also contributes to the conductivity of hybrids. Characterization of PAni blends using ac impedance by Passiniemi and Vakiparta

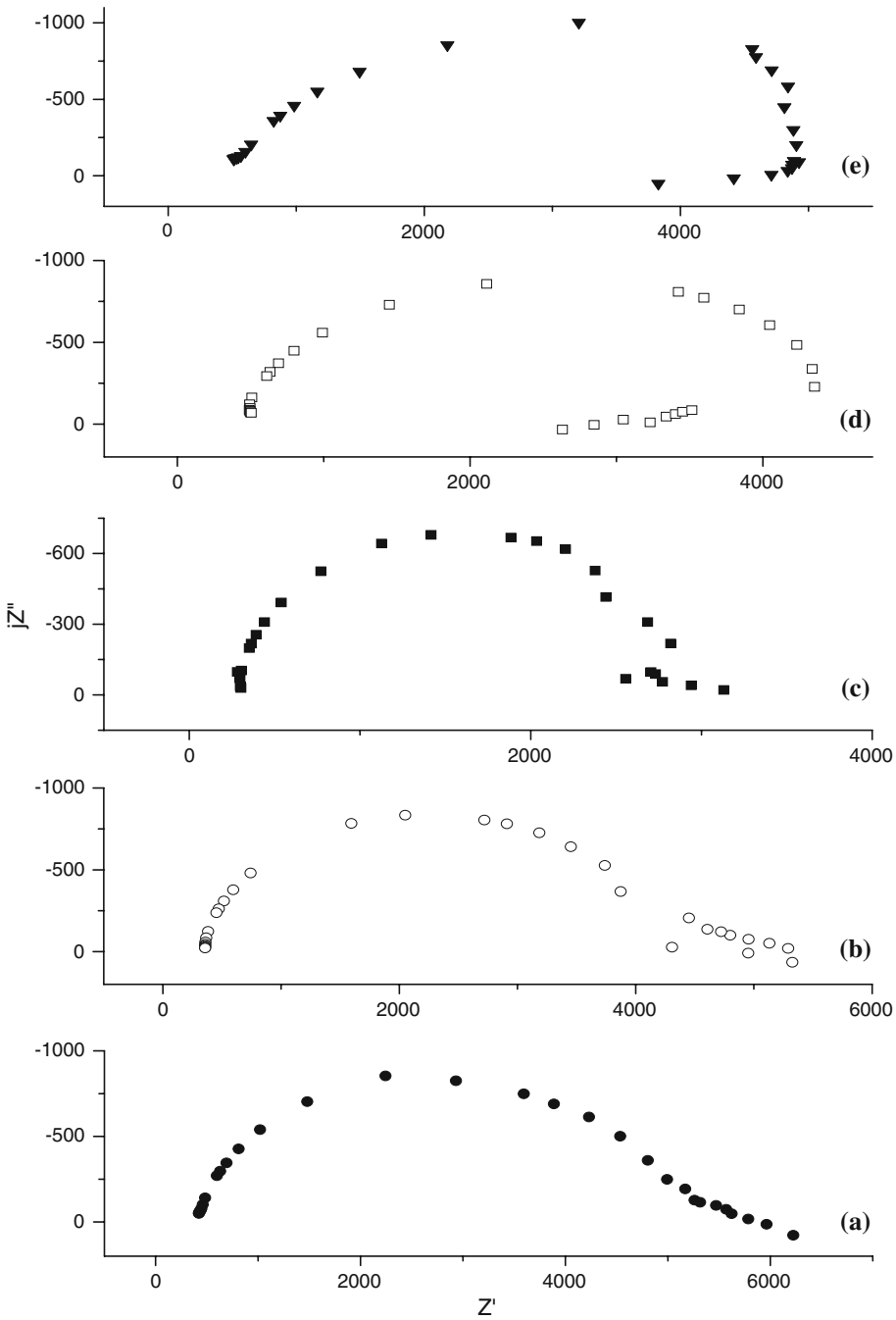

Fig. 6 Nyquist plots for P12MPA at temperatures **a** 300 K, **b** 323 K, **c** 348 K, **d** 373 K, and **e** 398 K

[23] also evidences that the resistance increases due to drying occurs in the resistance between conducting particle.

The relaxation frequency (f_0), relaxation time (τ), bulk capacitance (C_b), and bulk dielectric constant (ε_b) for PAni and PAniPOMs at room temperature are given in Table 3. On doping with polytungstate and polymolybdate, the relaxation time increases whereas it decreases on substituting vanadium in the dopant. The relaxation time is higher for P12TPA. This effect is visible in the bulk dielectric also.

The impedance spectra usually show semi circular arcs whose centers invariably lie below the real axis, inclined straight lines with finite slopes (spurs) or combinations of these. Often these arcs and spurs are sufficiently separated on a complex plane plot to allow easy graphical determination of the impedance parameters. In other instances, however, the impedance spectrum displays distortions of the various shapes constituting it because of overlapping time constants. Tsai and Whitmore [30] proposed a non-linear curve-fitting technique which allows fast, reliable, and accurate elucidation of the basic impedance parameters for cases having

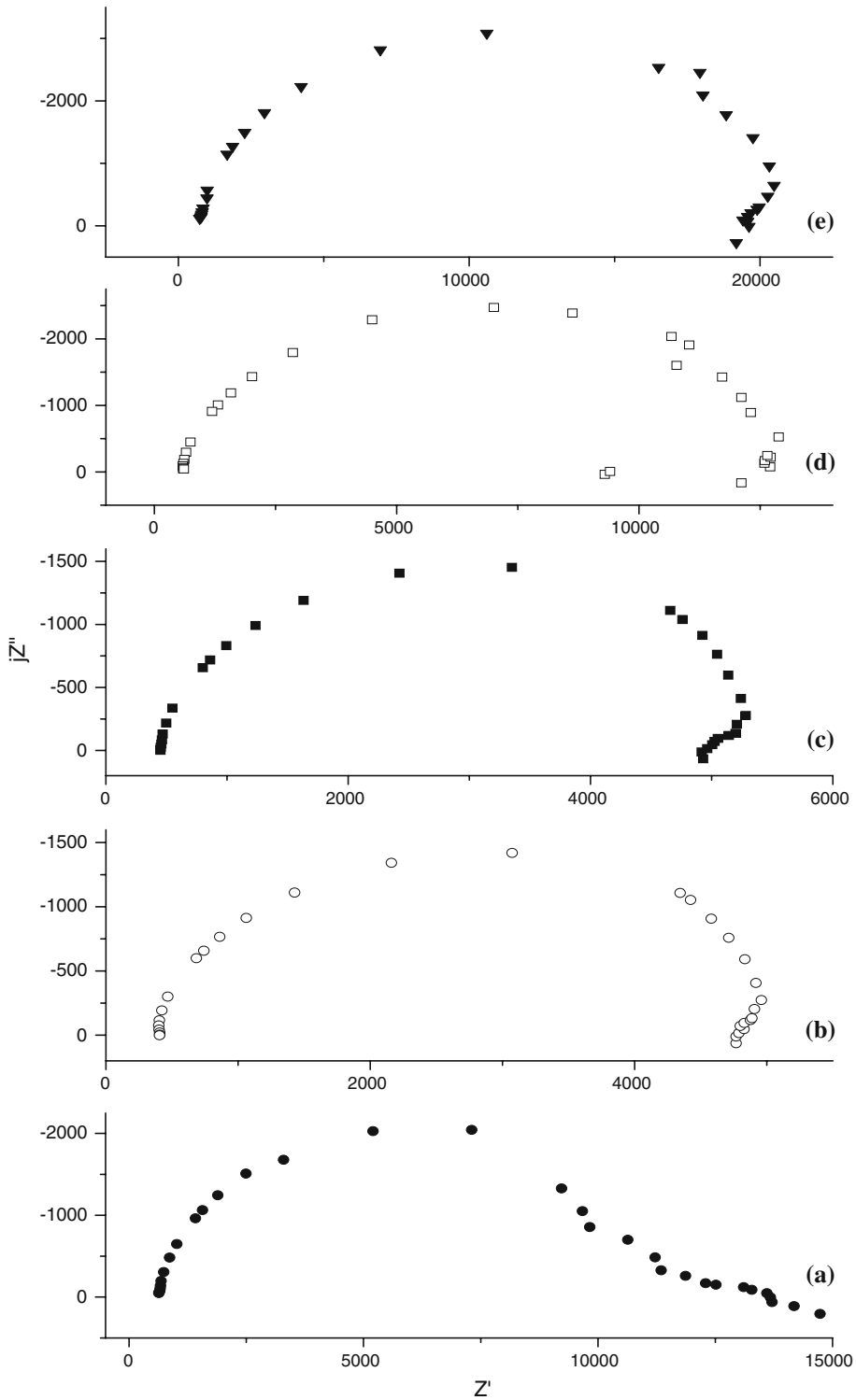

Fig. 7 Nyquist plots for P11MPA at temperatures **a** 300 K, **b** 323 K, **c** 348 K, **d** 373 K, and **e** 398 K

overlapping time constants. A depressed semi circle in the complex impedance plot as shown in Fig. 8 is described by an expression similar to Cole–Cole formula:

$$Z(\omega) = Z_\infty + (Z_0 - Z_\infty)/1 + (j\omega/\omega_0)^{(1-\alpha)} \quad (1)$$

where $Z(\omega)$ is the complex impedance at the angular frequency ω, Z_∞ the high frequency intercept of the arc with the real axis, Z_0 the low frequency real axis intercept, ω_0 the relaxation angular frequency, α the depression parameter ($0 \leq \alpha \leq ½$) and $j = \sqrt{-1}$. The limiting case of $\alpha = 0$ represents an equivalent circuit consisting of lumped R–C elements with a zero depression angle, while $\alpha = ½$ corresponds to a combination of resistors and Warburg impedance with a 45°depression angle. The equivalent

Table 3 Relaxation frequency (f_0), relaxation time (τ), bulk capacitance (C_b), and bulk dielectric constant (ε_b) of PAni and PAniPOMs at room temperature

Sample	f_0 (Hz)	τ (μs)	$C_b \times 10^{-8}$ (F)	$\varepsilon_b \times 10^4$ (F/m)
PAni	2000	80	1.57	1.338
P12TPA	600	265	25.71	21.915
P11TPA	1500	106	1.24	1.057
P12MPA	1000	159	2.77	2.361
P11MPA	2000	80	0.73	0.622

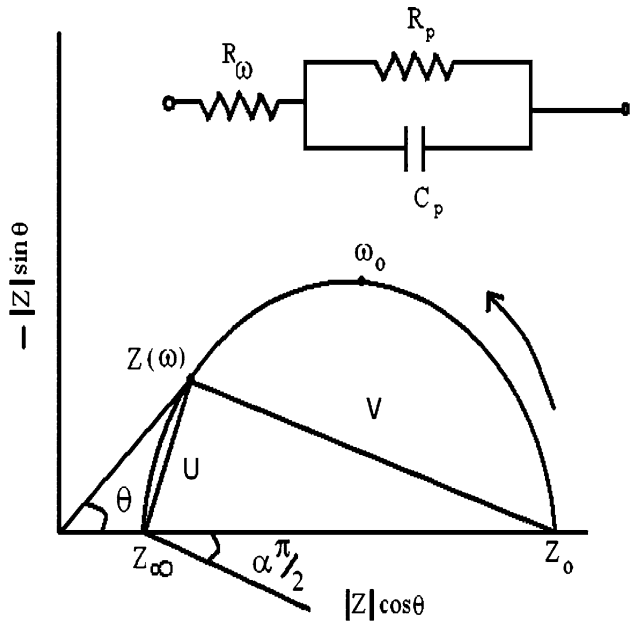

Fig. 8 Schematic complex impedance diagram, showing a semi circle whose center lies below the real axis

circuit corresponding to the impedance spectrum of Fig. 8 consists of a frequency dependant capacitor and two frequency independent resistors. By rearranging the above said equation, the relation obtained is,

$$\ln(V/U) = (1-\alpha)\ln\omega - (1-\alpha)\ln\omega_0 \quad (2)$$

where U and V are the distances of $Z(\omega)$ from Z_∞ and Z_0, respectively. A plot of ln $|V/U|$ vs. ln ω yields a straight line of slope $(1-\alpha)$. The depression angle α determined from the Nyquist plot is given in Table 2 for comparison. Generally, α lies between 0 and ½ for all the samples except for P12MPA and P11MPA above 373 K. The low value of α indicates the degree of depression of Nyquist semi circle arc and in turn the pseudocapacitance effect. The observed α value above 0.5 in P12MPA and P11MPA above 373 K supports the presence of two different phenomenons namely the grain boundary and the grain core at higher temperatures.

Frequency dependence of σ_{ac}

A frequency-dependant electrical conductivity $\sigma_{ac}(\omega)$ has been observed in many semiconductors, insulators and also in inorganic and polymeric organic materials. The charge transport measurements in these disordered solids will provide information about the electronic structure of the materials. The disorder in atomic configuration and/or composition causes localization of electronic states or groups of states with in the material. Since the charge carriers are localized, ac impedance techniques are used to examine such behaviors [31]. The frequency dependant conductivity has the form,

$$\sigma_{ac}(\omega) = A\omega^s \quad (3)$$

where ω is the angular frequency and the exponent s is less than or equal to unity. Usually, what is measured in an experiment is the total conductivity $\sigma_{tot}(\omega)$ of the sample at the particular frequency and temperature and can be written as,

$$\sigma_{tot}(\omega) = \sigma_{ac}(\omega) + \sigma_{dc} \quad (4)$$

where σ_{dc} is the dc conductivity. It is assumed that ac and dc conductivities are due to completely different processes. For example, σ_{ac} is due to hopping between defect centers and σ_{dc} is due to band conduction in extended states. When both processes are due to hopping between localized states, then σ_{ac} would arise from the carrier motion within isolated regions like voids, whereas σ_{dc} could arise from percolation channels established throughout the material. If these conditions are not met, and σ_{dc} is simply the $\omega \to 0$ limit of $\sigma_{ac}(\omega)$, then the separation given in Eq. 4 is no longer useful [32].

The ac conductivity of conducting polymers consists of frequency dependant behavior in the limit of low frequencies and a sub-linear response at higher frequencies [33]. The frequency dependence of ac conductivity for PAni and its hybrids in the high frequency region is obtained using the Eq. 3.

A plot of log ω vs. log σ_{ac} for PAni is shown in Fig. 9. The conductivity varies slowly at low frequencies and then increases fastly at high frequency region. The fractional dependence of ac conductivity upon frequency is found in many disordered materials and the exponential law (Eq. 3) arises from the many body interactions between hopping charges [34]. In other words it is due to the relaxation caused by the motion of electrons or ions, hopping or tunneling between equilibrium sites [35]. In such systems, the ac conductivity increases as the frequency increases, due to the contribution of charge carriers moving along smaller distances that is confined inside clusters. Thus, the frequency exponent, 's', expresses the relative reduction of clusters upon frequency. In the $s < 1$ region, $\sigma_{ac}(\omega)$

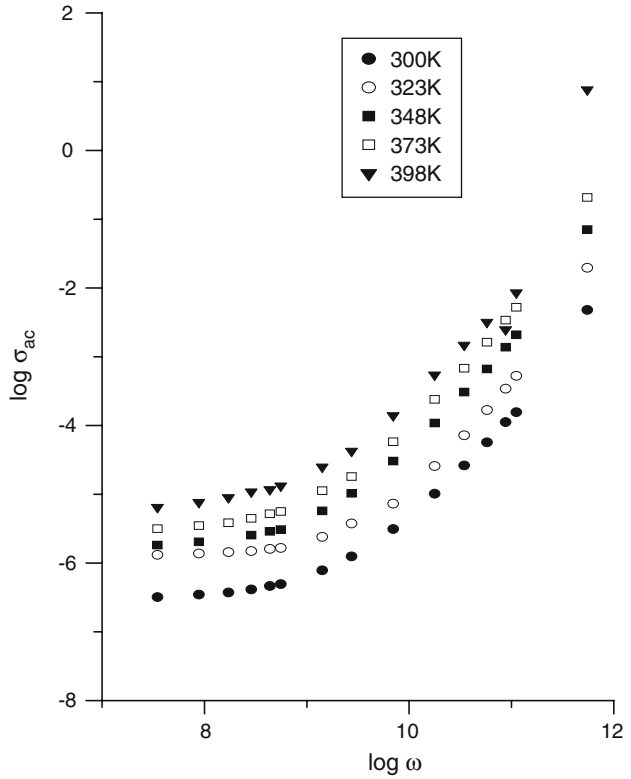

Fig. 9 Log–log plot of the conductivity at various temperatures for PAni

depends on temperature, while in the $1 < s < 2$ region, $\sigma_{ac}(\omega)$ is independent of temperature [36]. If hopping occurs between a random distribution of localized charge states, then s lies between 0.5 and 1. The lower value of s occurs for multiple hops while the higher value occurs for single hops [37].

In Fig. 9, a linear increase in conductivity with frequency is noticed in the region 100 Hz–20 kHz for PAni. The s parameter values are determined from the linear slope of log ω vs. log σ_{ac} for PAni at different temperatures, and are given in Table 2. The frequency exponent is a diagnostic tool for characterizing charge transport in conducting polymers. Exponents close to unity are associated with lattice response, while smaller values are due to impurities or dopant [32].

Figure 10a, b shows the plot of log ω vs. log σ_{ac} for P12TPA and P11TPA, respectively. A linear increase in conductivity is observed in the frequency region 100 Hz to 4.5 kHz for P12TPA and P11TPA. The exponent, s is determined from the slope of the linear region and is given in Table 2. Similarly the frequency dependant σ_{ac} plotted for P12MPA and P11MPA are shown in Fig. 11 and the s values are tabulated. As in disordered materials, the conductivity of these materials linearly increases with increasing frequency.

The electron tunneling model suggests that s is independent of T, but dependant of ω. In the case of small polaron tunneling, s increases with temperature, whereas for overlapping large polaron tunneling (OLPT), s decreases up to a certain temperature and then increases for further increase of temperature. In the correlated barrier hopping model (CBH), the s parameter value is below unity

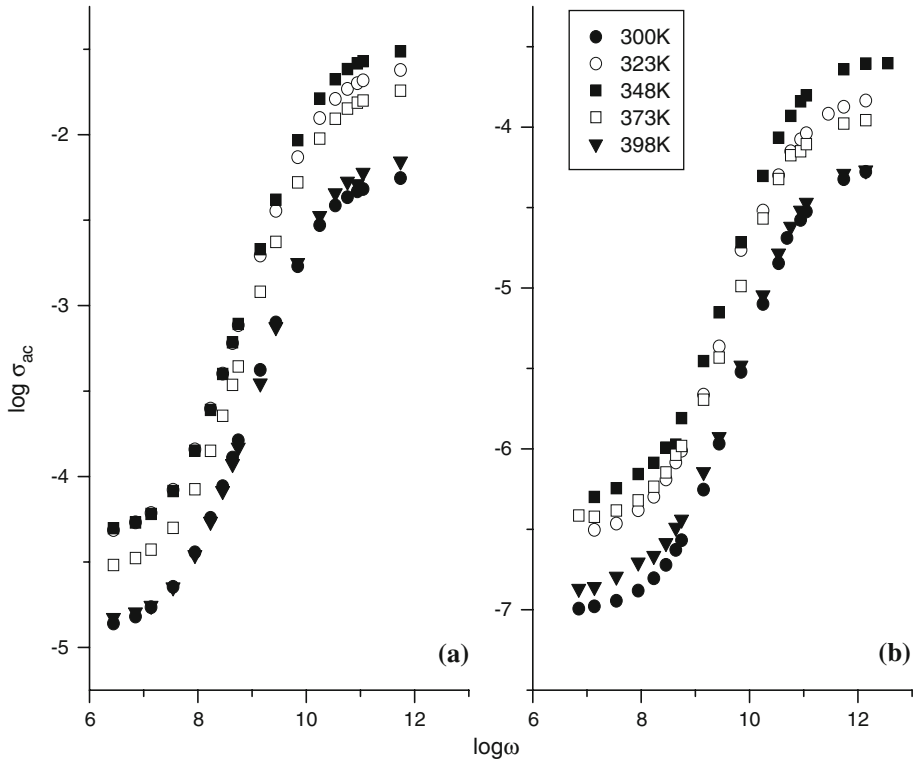

Fig. 10 Log–log plots of the conductivity at various temperatures for **a** P12TPA and **b** P11TPA

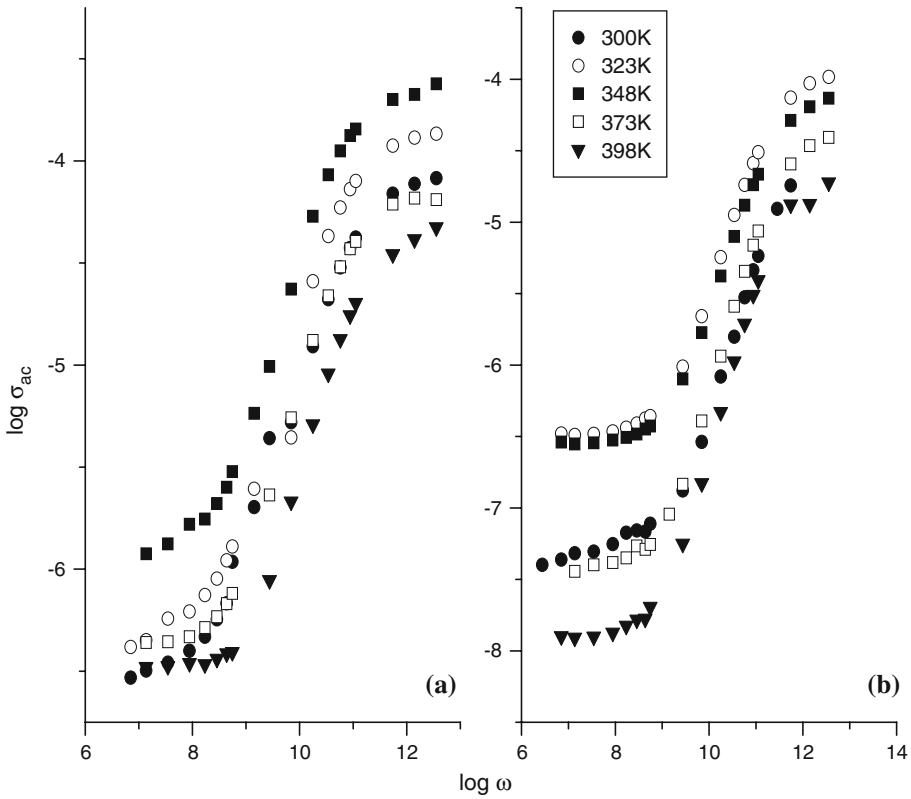

Fig. 11 Log–log plots of the conductivity versus frequency at various temperatures for **a** P12MPA and **b** P11MPA

and also decreases with increase in frequency. Pike [31] and Elliot [38] suggest that the charge carrier hops between defect sites D^+ and D^- over the potential barrier separating them [39]. According to Guintini et al. [40] each pair of D^+ and D^- is assumed to form a dipole with relaxation energy. This type of energy can be attributed to the existence of potential barrier over which the carriers hop [41].

The temperature dependence of *s* is shown in Fig. 12 and can be explained by various theoretical models for ac conductivity. In PAni, at room temperature the value of *s* close to unity is the evidence for weak interaction of polarons with the polymer backbone. At high temperatures, the thermal treatment has reduced the value of frequency exponent and affected the grain size and the inter-grain separation. The values of the frequency exponent for PAni are found to decrease with increasing temperature and the value of *s* parameter is below one which obeys the correlated barrier hopping model (CBH). The negative temperature dependence of the exponent s in CBH model arises due to the correlation between the barrier height and the hopping distance and this has an effect on the relaxation time.

In Fig. 12, the *s* parameter for P12TPA decreases upto a particular temperature and then increases for further increase of temperature, suggests the overlapping large polaron tunneling model (OLPT) might be a possible candidate. The observed low value of the frequency

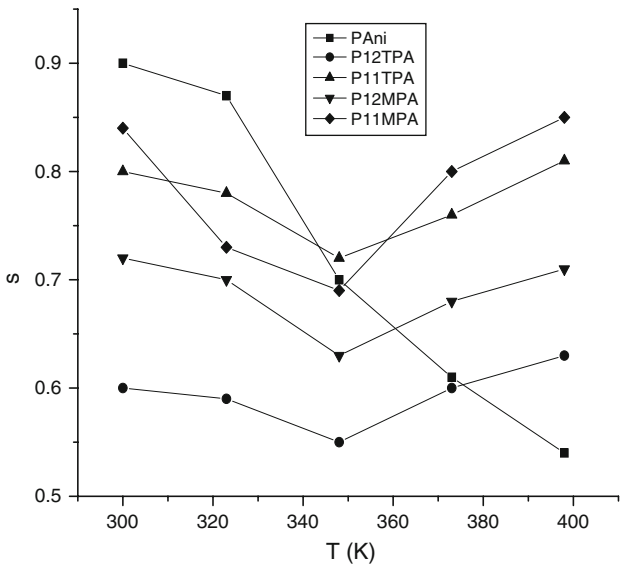

Fig. 12 A plot of temperature dependence of frequency exponent '*s*'

exponent compared to PAni at room temperature shows a strong interaction between polarons, polymer backbone, and polyanion. P11TPA, P12MPA, and P11MPA also show decrease of *s* upto 348 K and then an increase as temperature increases. The observed behavior of *s* for these materials suggests that the dominant conduction mechanism is OLPT.

A mechanism of quantum mechanical tunneling of large polarons with overlapping polaron wells predicts that $\sigma(\omega)$ should behave in some respect in a similar manner to CBH model, namely it should have a negative temperature dependence of s, at least at low temperatures. In OLPT, the large polaron wells of two sites overlap thereby reducing the value of the polaron hopping energy. At higher temperatures the s has positive temperature dependence in PAniPOM hybrids. This shows that, the thermally activated carriers and thermal vibrations of the nanomaterial might have given rise to the tunneling between the polymer and the polyoxometalate. The higher values of s obtained for polytungstates and polymolybdates on substitution of vanadium atom suggests single hop of polarons.

Conclusion

The number of water molecules in the POMs plays a vital role on the thermal stability of these organic/inorganic hybrid materials. The replacement of a tungsten addenda atom with a vanadium atom in P12TPA modifies the thermal stability of the hybrids. The impedance analysis results show that the addenda atom (vanadium) in the dopant polyoxometalate also contributes to the conductivity of PAni. Loss of water molecules, during dehydration, influence the conductivity of hybrids evidence the role of water molecule in the dopant. Due to the protonation of polymer at the electrode–electrolyte interface in the dehydration region, the pseudocapacitance is present in the Nyquist plot. The CBH model is obeyed by PAni while its hybrids obey the OLPT model due to inclusion of POMs.

Acknowledgements One of the authors P.C. would like to thank CSIR, New Delhi for a Senior Research Fellowship. The authors acknowledge Department of Atomic Energy—Board of Research in Nuclear Sciences, Mumbai for the financial assistance (Project No: 2006/34/28-BRNS).

References

1. Ross Macdonald J, Johnson WB (2005) In: Barsoukov E, Ross Macdonald J (eds) Impedance spectroscopy: theory, experiment and applications, 2nd edn. Wiley, Hoboken, NJ, p 1
2. Kivelson S (1981) Phys Rev Lett 46:1344
3. Bianchi RF, Leal Ferreira GF, Lepienski CM, Faria RM (1999) J Chem Phys 110:4602
4. White AM, Slade RCT (2003) Synth Met 139:123
5. Chithra lekha P, Balaji M, Subramanian S, Pathinettam Padiyan D (in press) Curr Appl Phys
6. Louis CW Baker, Diana C Glick (1998) Chem Rev 98:3
7. Nakamura O, Ogino I, Kodama T (1981) Solid State Ionics 3–4: 347
8. Doyle CD (1961) Anal Chem 3:77
9. Jeevananda T, Siddaramaiah (2001) Thermochim Acta 376:51
10. Bonanos N, Steele BCH, Butler EP (2005) In: Barsoukov E, Ross Macdonald J (eds) Impedance spectroscopy: theory, experiment and applications, 2nd edn. Wiley, Hoboken, NJ, p 205
11. Rudge A, Raistrick ID, Gottesfeld S, Ferraris JP (1994) Electrochim Acta 39:273
12. Bayhan M, Hashemi T, Brikman AW (1997) J Mater Sci 32: 6619. doi:10.1023/A:1018692101445
13. Hu C-C, Chen E, Lin J-Y (2002) Electrochim Acta 47:2741
14. Hu C-C, Lin J-Y (2002) Electrochim Acta 47:4055
15. Xiao Q, Zhou X (2003) Electrochim Acta 48:575
16. Darowicki K, Kawula J (2004) Electrochim Acta 49:4829
17. White AM, Slade RCT (2003) Electrochim Acta 48:2583
18. Koleli F, Ropke T, Hamann CH (2003) Electrochim Acta 48: 1595
19. Hu C-C, Chu C-H (2001) J Electroanal Chem 503:105
20. Liu X-X, Li Y-B, Bian L-J, Dou Y-Q, Huo Y-Q (2008) J Solid State Electrochem 12:909
21. Kulkarni MV, Viswanath AK (2005) Sens Actuators B 107:791
22. McGovern ST, Spinks GM, Wallace GG (2005) Sens Actuators B 107:657
23. Passiniemi P, Vakiparta K (1995) Synth Met 69:237
24. Maier J (1986) Ber Bunsenges Phys Chem 90:26
25. Sunde S (2000) J Electroceram 5:153
26. Jain S, Chakane S, Samui AB, Krishnamurthy VN, Bhoraskar SV (2003) Sens Actuators B 96:124
27. Bishop A, Gouma P (2005) Rev Adv Mater Sci 10:209
28. Mioc U, Davidovic M, Tjapkin N, Colomban Ph, Novak A (1991) Solid State Ionics 46:103
29. Agbor NE, Petty MC, Monkman AP (1995) Sens Actuators B 28:173
30. Tsai Y-T, Whitmore DH (1982) Solid State Ionics 7:129
31. Pike GE (1972) Phys Rev B 6:1572
32. Extance P, Elliot SR, Davis EV (1985) Phys Rev B 32:8148
33. Papathanassiou AN, Sakellis I, Grammatikakis J, Vitoratos E, Sakkopoulos S, Dalas E (2004) Synth Met 142:81
34. Bilen B, Skarlatos Y, Aktas G (2005) J Non-Cryst Solids 351: 2153
35. Ammar AH, Farag E-SM, El-Ocker MM (2007) J Mater Sci: Mater Electron 18:469
36. Waki H, Kawamura J, Kamiyama T, Nakamura Y (2002) J Non-Cryst Solids 297:26
37. Prabakar K, Narayandass SK, Mangalraj D (2003) Mater Chem Phys 78:809
38. Elliot SR (1977) Philos Mag 36:1291
39. Farid AM, Bekheet AE (2000) Vacuum 59:932
40. Guintini JC, Zanchetta JN, Jullien D, Enolie R, Houenou P (1981) J Non-Cryst Solids 45:57
41. Abou El-Hassan S, Hammad M (2001) Phys Status Solidi A 185: 413